A Wideband Dipole Antenna Design for Through-the-Wall Imaging on Security Applications

Joof, Sulayman ; Doğu, Semih ; Çelik, Feza Turgay; Karaçuha, Kamil

DOI
10.23919/EuCAP57121.2023.10133780

Publication date
2023

Document Version
Final published version

Published in
Proceedings of the 2023 17th European Conference on Antennas and Propagation (EuCAP)

A Wideband Dipole Antenna Design for Through-the-Wall Imaging on Security Applications

Sulayman Joof*, Semih Doğu †, Feza Turgay Çelik‡, Kamil Karaçuha§
*Department of Communication Systems, Istanbul Technical University, Istanbul, Türkiye
† Department of Electronics and Communication Engineering, Istanbul Technical University, Istanbul, Türkiye
‡Department of Microelectronics, Delft University of Technology, Delft, Netherlands, F.T.Celik@tudelft.nl*
§Department of Electrical Engineering, Istanbul Technical University, Istanbul, Türkiye

***Abstract*—This study proposes a dipole antenna with wide-band characteristics for microwave imaging (MWI) applications. The wide-band characteristic of the antenna is achieved by reshaping the geometry of the conventional dipole. The dipole is fed by a specially designed balun, together with a ground reflector in order to obtain a high gain unidirectional pattern. The antenna is operating from 2.7 to 5 GHz with a maximum realized gain of 8.39 dBi and $|S_{11}|$ less than -10 dB within this frequency band. The simulation results and evolution of the design procedure are provided. Furthermore, a through-the-wall MWI scenario consisting of thirteen antenna elements, a concrete wall, and two hidden objects behind the wall is implemented to evaluate the performance of the antenna. The 2-D reconstruction results obtained from inversion methods indicate that the proposed antenna is a potential candidate for through-the-wall MWI applications.**

***Index Terms*—broadband antenna, enhanced dipole antenna, Microwave imaging (MWI)**

I. Introduction

The present study aims to design a bandwidth-enhanced dipole antenna structure and employ the corresponding design in a microwave imaging application. Throughout the study, important parameters of both the antenna structure and microwave imaging are analyzed and presented. To obtain enhanced impedance and radiation bandwidth, specialized balun and flared structures are utilized by taking into account the current paths in the operating frequency band. In this study, a microwave imaging system is studied to detect objects behind the wall. The antenna part of the system will be discussed in this chapter. Microwave imaging systems work with forwarding and inverse problem ideas, so the antenna system is used to add a transmitter for the forward problem while they operate as a receiver for the reverse problem. To increase the imaging capability of the system, broadband and linearly polarized antennas should be used for this application. Most of the popular imaging system employs printed Vivaldi type antenna for such application: however, printed Vivaldi antenna has several problems. One of these problems is the size of the Vivaldi antenna. Vivaldi antenna has a large electrical size in its aperture plane, which limits the arraying options of this antenna. The second problem of the Vivaldi antenna can be seen as its cross-polarization. Printed Vivaldi antennas have a flared aperture, this aperture causes polarization direction differences between different frequencies in the operating region [1]. The last important drawback of the Vivaldi antennas is their mutual coupling performance in array structures. When a Vivaldi 2-D array is formed, the coupling between elements is inevitable. The excess amount of the coupling makes the design and simulation process of the 2D Vivaldi arrays extremely costly. In this paper, we suggest a broadband printed dipole antenna instead of a printed Vivaldi antenna to overcome the drawbacks mentioned above.

The effectiveness of the proposed antenna is demonstrated with a through-the-wall (TWI) microwave imaging example. TWI applications are including but are not limited to searching firearms, tracking people for rescue operations, and locating the position of pipes behind the wall [2]–[5]. In TWI scenarios, mostly, reconstructing only the shape and the position of the objects is aimed due to the existence of the wall, which has the feature of absorbing electromagnetic fields and preventing them to reach the objects hidden behind the wall. Fast response from imaging methods is also required to fulfill the goal of the TWI applications. Therefore, to produce the image of the area behind the wall, the linear sampling method (LSM) is utilized [6], [7]. The presented results prove the capability of the proposed antenna for a TWI scenario.

II. Wide-Band Dipole Antenna Design

A. The Antenna Configuration

In our design, we evolved a simple dipole antenna into a wide-band dipole antenna suitable for MWI applications. Fig. 1 shows the top view configurations of the evolved dipole geometries named Antenna I, II, and III, respectively.

Broadband printed dipole antenna is designed to evolve from a regularly printed dipole antenna. In a regular dipole antenna, the arms of the structure are realized on different layers and feeding is done by using a microstrip-line structure. The top view of the regularly printed dipole can be seen in Fig. 1 as Antenna I [8]. In imaging systems, high gain in the radiation pattern is another requirement: therefore, a ground plane needs to be added in the second layer of the antenna. This requirement pushed dipole to be realized in a single layer and the design evolved to the Antenna II (Fig. 1). This antenna needs to be fed with a probe-type connection. Since this connection creates a passage from an unbalanced

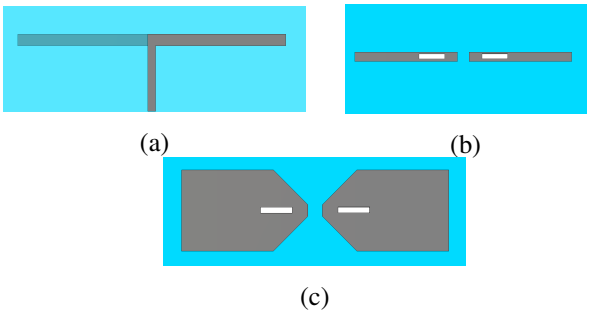

Fig. 1: Top views of the (a) Antenna I, (b) Antenna II, and (c) Antenna III.

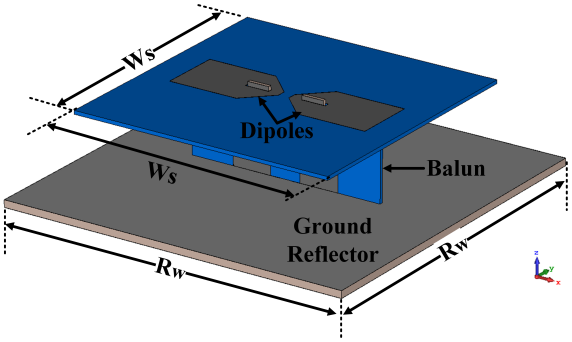

Fig. 3: Final configuration of the proposed dipole filtering antenna (Antenna III).

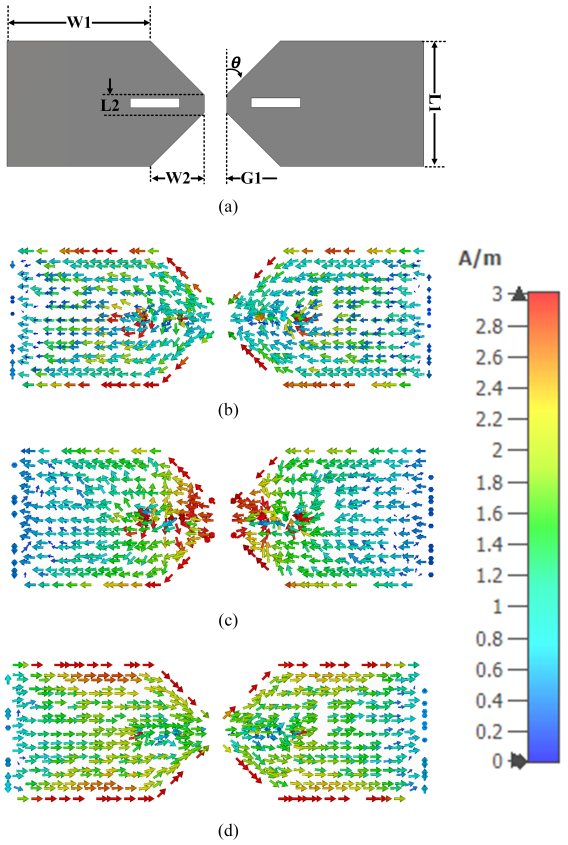

Fig. 2: Antenna III: (a) Top-view of dipole. Surface current at (a) 2.6 GHz, (b) 3.6 GHz, and 5 GHz.

to a balanced structure, after this point our designs need a Balun structure. Antenna II illustrates 15% bandwidth which is not enough to realize imaging with low error. Therefore, the design is elevated to Antenna III to achieve large impedance and radiation pattern bandwidth [9]. The top view and the isometric view of Antenna III can be seen in Fig. 2 and Fig. 3, respectively. Antenna III is designed by preserving the radiation characteristics of the antenna. The main idea of the design is to provide various paths to the surface currents [10]. Nevertheless, the essential point of the design is to preserve the behavior of the surface currents. They must start from the ends of the antenna and flow toward the feeding point. Any difference in the current path will result in a difference in the polarization direction; therefore, the only current paths are changed, not their directions. To fulfill the requirement on the surface current mentioned above, a wide-printed dipole strip is developed [9]. This antenna increases the bandwidth with a similar idea as the bow-tie structure but it outperforms the bow-tie in bandwidth considerations. This design uses a thick dipole; therefore, it has more different current path options that are possible with the bow-tie structure. Also, Antenna III guides the surface currents according to its dipole nature, so the polarization direction of all operating frequencies is the same. The surface currents of different frequencies can be seen in Fig. 2. As can be seen from these figures, the surface currents of the antenna follow the same route. The antenna has three major parameters that plays important role in its radiation characteristic and so bandwidth. The important Parameters of the antenna can be seen in Fig. 2(a) as L1, G1, and, θ.

The final configuration of the antenna consists of a ground reflector and a balun as depicted in Fig. 4. The balun is composed of a Γ-shaped microstrip feed line, a slot line formed by two patches located on the ground side of the substrate, and a shorted stub. As described in [11], the slot line coupled by the Γ-shaped microstrip line excites the dipoles. In addition, a more realistic simulation is achieved by connecting a 50Ω SMA connector to a Γ-shaped microstrip feed line. By selecting appropriate geometric parameters, the antenna element is able to exhibit good wideband performance. Optimized values for the geometric parameters of the final antenna configuration are provided in Table I. It should be highlighted that both the dipole and Balun were printed on a Rogers 4003 substrate, with relative permittivity and thickness of 3.55 and 0.8 mm, respectively. The simulations were performed with CST Microwave Studio.

B. Effect of the Parameters (L1, G1, and θ) on the Performance of the Antenna

The parameter L1 defines the width of the antenna. The general concept of a thick dipole is as follows; the more we increase the L1, the more bandwidth we can get. This idea

TABLE I: Dimensions of the proposed antenna

Parameter	Value(mm)	Parameter	Value(mm)
G1	2.5	W2	5
L1	14	W4	4
L3	2	W5	8
L4	17	W6	4
L5	3	W7	7
L6	4	W8	14
L7	5	W9	6.5
L8	5	W10	8
L9	3.5	W11	5
L10	1.81	W12	3.9
L11	12.4	W13	45
L12	2	W14	10
L13	1.3	W15	12
L14	0.3	W16	0.2
Rw	80	W17	1.2
Ws	60	W18	1
W1	16.97	θ(deg)	45

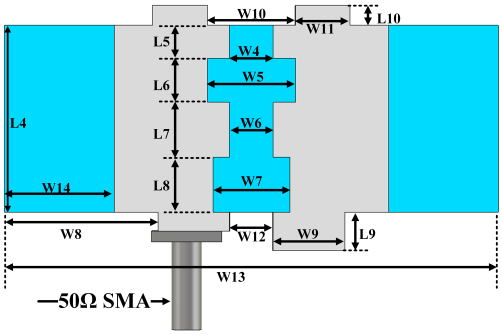

(a)

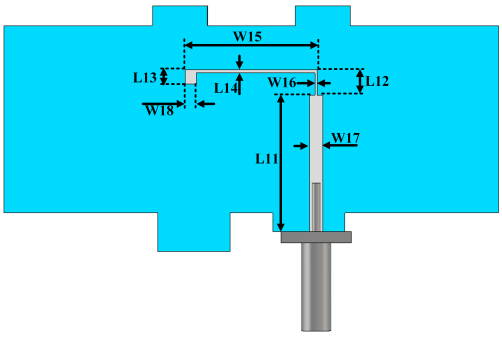

(b)

Fig. 4: (a) Ground and (b) feed side of the balun.

generally holds as it can be seen from $|S_{11}|$ performance of the antenna under different L1 conditions as seen in Fig. 5(a).

Another important antenna parameter was the G1 value of the antenna. This value represents the distance between dipole arms, and it plays important role in the impedance characteristics. The effect of G1 on $|S_{11}|$ value can be seen in Fig. 5(b). The lower G1 value stabilizes the input impedance and reflection parameter of the antenna as seen in the figure.

The third important antenna parameter that has a huge impact on the bandwidth of the antenna is the flare angle of the dipole (θ). Large bandwidth can be obtained by creating very different current paths on the antenna, so the large flare angles provide much more bandwidth [9]. The effect of θ on the $|S_{11}|$ can be seen in Fig. 5(c). When the transition from the feeding point and the edge are sharp, surface currents are also excited for the higher frequencies. The graph belonging to the θ=60^0 variations excites the highest frequency compared to the other variations, so the highest scan angles seem to be more beneficial in terms of bandwidth. Even though the antenna parameters L1, G1, and θ can be adjusted to get large bandwidth, they have limitations due to radiation pattern bandwidth. The parameters are selected to provide both large impedance and radiation pattern bandwidth. The values of these critical dimensions can be found in Table I.

As a unidirectional antenna with high-gain properties is essential for through-the-wall microwave imaging applications, a ground plane reflector is employed to attain this requirement. The simulated maximum realized gain of the proposed antenna with respect to frequency is provided in Fig. 6(a). Additionally, the configuration of MWI applications generally requires multiple antennas in an array format. Fig. 6(b) demonstrates the S-parameters of an array including 13 of the proposed antenna element separated by a distance of 2 cm between two adjacent ground plane and 10 cm between two ports. The results in Fig. 6(b) show that the antennas possess similar reflection coefficient characteristics while maintaining negligible coupling between the antenna elements within its impedance bandwidth. After investigating the important antenna parameters, the optimum dimensions are selected and presented in Table 1.

III. Through-the-Wall Imaging Application

The usage of the designed antenna is investigated in a through-the-wall microwave imaging scenario by employing CST simulations. To optimize the effectiveness of the antennas, the distance d between the antennas and the wall is studied. One antenna is placed on one side of the wall and the magnitude of electric field values at the dominant polarization's direction (at z direction) is measured on the other side of the wall. The probed area is 20 cm by 30 cm with 5 cm and 6 cm separations at the x and y axis, respectively. The distance d is varied from 1 mm to 70 mm and this configuration is given in Fig. 7(a). The operating frequency is swept from 2.6 GHz to 5 GHz with 50 MHz steps. The wall has a 10 cm thickness in the y direction and covers the whole x and z directions. Its dielectric material is selected from the CST library under name of *concrete wall (1-year-old)*. The measured electric field values are averaged over sampling points and the operating frequencies. The corresponding results are plotted in Fig. 7(b) for the various d values and the highest electric field strength is achieved at $d = 16$ mm.

Next, an antenna array, which consists of 13 proposed antennas, is constructed and placed on one side of the wall as previously mentioned. Two perfect electric conductor cylinders

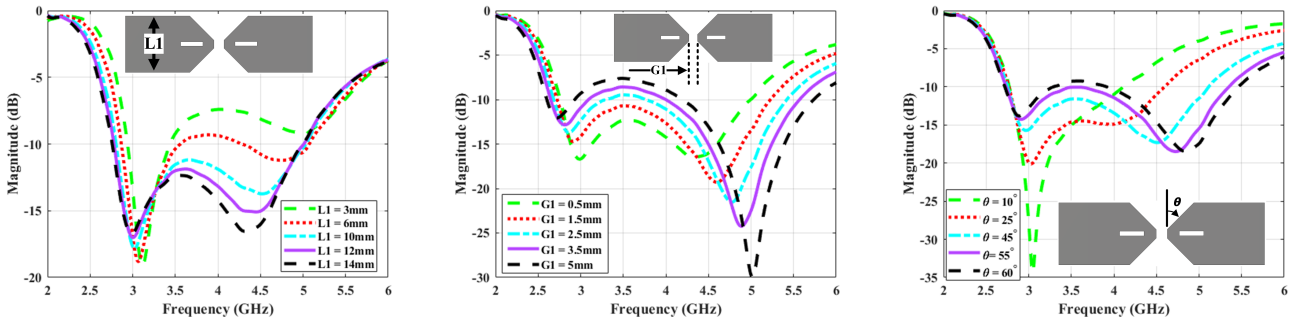

(a) (b) (c)

Fig. 5: Effect of the Parameters (L1, G1, and θ). (a) Effect of L1 on the $|S_{11}|$ parameter of the dipole antenna (L1 = 14mm bandwidth = %57.73). (b) Effect of G1 on the $|S_{11}|$ parameter of the dipole antenna. (c) Effect of θ on the $|S_{11}|$ parameter of the dipole antenna.

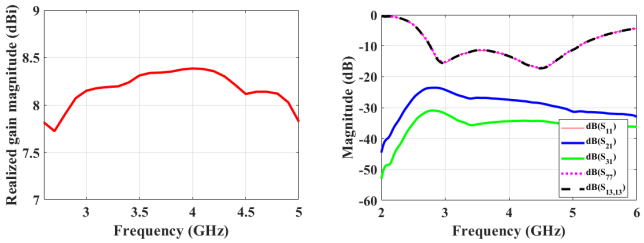

(a) (b)

Fig. 6: (a) Maximum realized gain over frequency. (b) S-parameters of the proposed antenna array with 13 antenna elements.

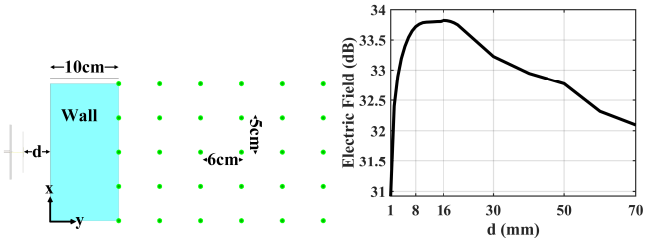

(a) (b)

Fig. 7: (a) Probe locations. (b) Magnitude of received electric field strength with respect to parameter d.

with a radius of r1=6 cm and r2=4 cm are positioned on the other side of the wall and both cylinders are 10 cm in length. The array antenna aperture is 120 cm at the x-axis and the distance between two subsequent antennas' extends is 2 cm. This configuration is given in Fig. 8(a). Two measurements are performed in the presence and the absence of the targets. The difference between these data is employed to reconstruct the image of the area behind the wall.

In this study, the linear sampling method (LSM), which finds an indicator to depict the shape and locations of the targets, is employed and a piece of brief information is given.

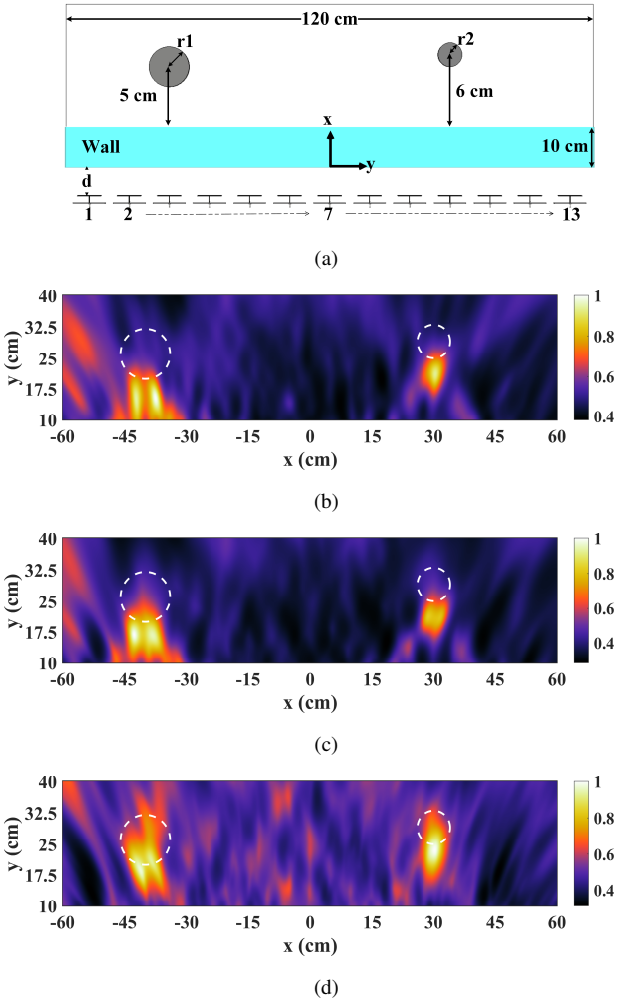

(a) (b) (c) (d)

Fig. 8: (a) Through-the-wall imaging configuration. Normalized LSM indicator for (b) $d = 1$ mm, (c) $d = 16$ mm and (d) $d = 70$ mm. Exact borders of the objects are marked with white dashed lines.

We refer to [6], [7] for details about the LSM. The indicator of the LSM is given as:

$$I(r) = \frac{1}{N_f} \sum_{f=1}^{N_f} \frac{||g_f(r,r')||^{-1}_{L_2(\Gamma)}}{\max ||g_f(r,r')||^{-1}_{L_2(\Gamma)}} \quad (1)$$

where g_f indicates the solution of LSM equation at each operating frequency:

$$\int_\Gamma S(r',r'')g_f(r,r')d\Gamma(r') = G(r'',r). \quad (2)$$

Here, r, $r' \in \Gamma$, and r'' are the locations of sampling points of LSM, transmitting antennas, and receiving antennas, respectively. S is the differential scattering parameter measurements and G stand for the free space's Green's function.

In order to demonstrate the effectiveness of the LSM results with respect to the parameter d, three different cases are investigated for $d = 1$ mm, $d = 16$ mm, and $d = 70$ mm. The indicator of (1) is normalized with respect to its maximum value and plotted for these cases in Fig. 8(b), 8(c), and 8(d) respectively. As seen from these figures, the best-reconstructed image with less noise is obtained at $d = 16$ mm. Note that, a slight error in the exact position of the cylinders is observed due to not employing the exact Green's function of the problem. The results indicate that the proposed antenna can be suitable for practical through-the-wall microwave imaging applications.

IV. Conclusion

This work presents the design of a dipole antenna with wideband properties for microwave imaging (MWI) applications. The design procedure includes the evolution of the antenna from its conventional configuration to a dipole antenna with high gain and wideband characteristics. The initial design phase is the parametric study of some important parameters such as the distance between dipole arms, flare angle, and width of the dipole which mainly affects the bandwidth of the antenna. This is followed by the design of the balun to excite the dipoles and to provide support between the ground reflector and the dipole substrate. The ground reflector is added to the design to provide high-gain uni-directional radiation properties. The final proposed antenna has an impedance bandwidth of at least 59%. Furthermore, the performance of the proposed antenna is tested in a through-the-wall MWI application. The imaging scenario includes 13 elements of the proposed antenna placed on one side of the concrete wall and two metallic cylinders on the other side. At first, the amount of electric field strength received behind the wall with respect to the distance of the antenna to Wall (d) when a single antenna is excited is studied. They indicated that the highest electric field strength is received at $d = 16$ mm. Based on this observation, three different imaging scenarios at for $d = 1$ mm, $d = 16$ mm, and $d = 70$ mm is investigated. The LSM-based imaging scheme detected the cylinders with the best-reconstructed image obtained when is $d = 16$ mm. Finally, the obtained results demonstrated that the proposed antenna can be a part of a real experimental set-up for through-the-wall MWI application.

Acknowledgement

This study is supported by ITU BAP under project 44280.

References

[1] E. M. Yıldız, C. F. G. Dede, K. Karaçuha, and S. Eker, "A gain enhancement study on a vivaldi antenna for radar applications," in *2022 IEEE International Symposium on Antennas and Propagation and USNC-URSI Radio Science Meeting (AP-S/URSI)*, 2022, pp. 1218–1219.

[2] S. Doğu, İ. Dilman, A. O. Ertay, and A. Uysal, "Modified printed monopole antenna with well-matched impedance bandwidth for through the wall microwave imaging applications," in *2020 28th Telecommunications Forum (TELFOR)*, 2020, pp. 1–4.

[3] A. Fedeli, M. Pastorino, C. Ponti, A. Randazzo, and G. Schettini, "Forward and inverse scattering models applied to through-wall imaging," in *2020 14th European Conference on Antennas and Propagation (EuCAP)*, 2020, pp. 1–4.

[4] A. Randazzo, C. Ponti, A. Fedeli, M. Pastorino, and G. Schettini, "A hybrid lebesgue-space inverse-scattering technique for microwave imaging of objects hidden behind a wall," in *2022 16th European Conference on Antennas and Propagation (EuCAP)*, 2022, pp. 1–5.

[5] S. Dogu and M. N. Akinci, "Assessment of linear sampling method and factorization method for through the wall imaging," in *2018 26th Telecommunications Forum (TELFOR)*, 2018, pp. 420–425.

[6] D. Colton, H. Haddar, and M. Piana, "The linear sampling method in inverse electromagnetic scattering theory," *Inverse Problems*, vol. 19, no. 6, pp. S105–S137, nov 2003.

[7] S. Doğu, M. N. Akınci, and E. Gose, "Experimental moving target imaging in a nonanechoic environment with linear sampling method," *IEEE Geoscience and Remote Sensing Letters*, vol. 18, no. 3, pp. 441–445, 2021.

[8] J.-M. Floc'h, A. E. S. Ahmad, J.-M. Denoual, and H. Rmili, "Design of printed dipole antenna with reflector and multi-directors," *International Journal on Communications Antenna and Propagation*, vol. 2, no. 6, pp. 407–413, 2012.

[9] L. Alatan, "Wideband omnidirectional and sector coverage antenna arrays for base stations," *Progress In Electromagnetics Research C*, vol. 82, pp. 29–38, 2018.

[10] F. T. Çelik and K. Karaçuha, "A conical-beam dual-band double aperture-coupled stacked elliptical patch antenna design for 5g," *Turkish Journal of Electrical Engineering and Computer Sciences*, vol. 30, no. 6, pp. 2073–2085, 2022.

[11] Y. Gou, S. Yang, J. Li, and Z. Nie, "A compact dual-polarized printed dipole antenna with high isolation for wideband base station applications," *IEEE Transactions on Antennas and Propagation*, vol. 62, no. 8, pp. 4392–4395, 2014.